Available online at www.sciencedirect.com
SCIENCE DIRECT®
Biomaterials 26 (2005) 63–72
Biomaterials
www.elsevier.com/locate/biomaterials

The effect of PEGT/PBT scaffold architecture on the composition of tissue engineered cartilage

J. Malda[a,b,c,*], T.B.F. Woodfield[a,b], F. van der Vloodt[a,c], C. Wilson[d], D.E. Martens[c], J. Tramper[c], C.A. van Blitterswijk[a,b], J. Riesle[a]

[a] *IsoTis S.A., Bilthoven, The Netherlands*
[b] *Institute for Biomedical Technology (BMTI), University of Twente, Enschede, The Netherlands*
[c] *Food and Bioprocess Engineering Group, Wageningen University, Wageningen, The Netherlands*
[d] *Department of Orthopaedics, University Medical Center, Utrecht, The Netherlands*

Received 1 September 2003; accepted 2 February 2004

Abstract

A highly interconnecting and accessible pore network has been suggested as one of a number of prerequisites in the design of scaffolds for tissue engineering. In the present study, two processing techniques, compression-molding/particulate-leaching (CM), and 3D fiber deposition (3DF), were used to develop porous scaffolds from biodegradable poly(ethylene glycol)-terephthalate/poly(butylene terephthalate) (PEGT/PBT) co-polymers with varying pore architectures. Three-dimensional micro-computed tomography (μCT) was used to characterize scaffold architectures and scaffolds were seeded with articular chondrocytes to evaluate tissue formation. Scaffold porosity ranged between 75% and 80%. Average pore size of tortuous CM scaffolds (182 μm) was lower than those of organized 3DF scaffolds (525 μm). The weight ratio of glycosaminoglycans (GAG)/DNA, as a measure of cartilage-like tissue formation, did not change after 14 days of culture whereas, following subcutaneous implantation, GAG/DNA increased significantly and was significantly higher in 3DF constructs than in CM constructs, whilst collagen type II was present within both constructs. In conclusion, 3DF PEGT/PBT scaffolds create an environment in vivo that enhances cartilaginous matrix deposition and hold particular promise for treatment of articular cartilage defects.

Keywords: Chondrocytes; Cartilage tissue engineering; Scaffold; Cell culture; In vitro; In vivo

1. Introduction

Tissue engineering holds promise for revolutionary advances in health care and considerable efforts have been directed towards the development of autologous substitutes to regenerate, maintain, or improve tissue and organ function. None more so than articular cartilage (AC), a connective tissue which, when damaged, exhibits limited intrinsic regenerative capacity [1]. In general, tissue-engineered constructs require a highly porous artificial extra-cellular matrix (ECM) or scaffold material to accommodate mammalian cells and to organize tissue regeneration in a three-dimensional (3D) environment. Nevertheless, limitation in the diffusion of nutrients has been suggested as a cause for the inhomogeneous neo-cartilage distribution observed in larger tissue-engineered cartilaginous constructs, whereby, the onset of chondrogenesis occurs solely within the peripheral boundaries [2–5]. Indeed, it has been demonstrated that nutrient gradients, such as oxygen in particular [5,6], can be measured and do occur within these tissue-engineered constructs. Therefore, in an effort to improve nutrient transport to cells, there has been considerable interest in the development of bioreactors in which medium flow is applied [7–9], or which mimic the periodic compressive stresses within articulating joints [10,11]. Although these dynamic culture conditions typically result in an improved quality of the neo-cartilage tissue formed, the 3D pore architecture present within scaffolds used for cartilage tissue engineering also likely has a large influence on tissue formation.

While several investigators [12–14] have evaluated the effect of scaffold pore size on cartilage tissue formation,

*Corresponding author. Department of Polymer Chemistry and Biomaterials, University of Twente/IsoTis S.A., P.O. Box 98, 3720 AB Bilthoven, Netherlands.
E-mail address: jos@malda.nl (J. Malda).

0142-9612/$ - see front matter © 2004 Elsevier Ltd. All rights reserved.
doi:10.1016/j.biomaterials.2004.02.046

to the best of our knowledge, pore architecture was not investigated systematically. In characterizing porous materials it is common practice to quote an average pore size or a pore-size distribution [12]. While these are important characteristics, particularly for controlling mechanical properties, pore accessibility and the pore tortuosity are, next to the porosity, of great significance for minimizing diffusional constraints and ultimately for successful tissue-engineering applications [15–19].

In this study we wanted to more closely evaluate the effect of a pore architecture, and more specifically, pore accessibility, on the composition of tissue-engineered cartilage. Therefore, careful design and characterization of porous scaffolds was necessary. The two most commonly used scaffold architectures reported in the literature for cartilage repair are porous sponges and non-woven fiber meshes [20]. At present, we are evaluating a series of amphiphilic, biodegradable poly (ether ester) multiblock copolymers as carrier materials for AC repair. The co-polymers are based on hydrophilic poly(ethylene glycol)-terephthalate (PEGT) and hydrophobic poly(butylene terephthalate) (PBT) blocks. Varying the amount and the length of the PEGT and PBT blocks offers extensive possibilities in the design of polymer systems with tailor-made properties, such as swelling, degradability and mechanical strength, as reported previously [21–24].

Two porous PEGT/PBT scaffold architectures were evaluated herin; a compression-molded/particle-leached sponge (CM), and a novel 3D-deposited fiber (3DF) scaffold. By accurately controlling the two processing techniques, the aim was to produce scaffolds with the same bulk composition and overall porosity, but different pore geometries. Scaffold architecture was then comprehensively characterized and cartilage tissue formation was evaluated on cell-seeded constructs maintained in vitro and in vivo.

2. Materials and methods

2.1. Scaffold preparation

PEGT/PBT co-polymers were obtained from IsoTis S.A. (Bilthoven, The Netherlands). Two scaffolds with different architecture were produced from PEGT/PBT resin with a PEG molecular weight of 300 g/mol and a PEGT:PBT weight percentage ratio of 55:45.

CM scaffolds (Figs. 1A and C) were prepared using a compression molding and particle-leaching method as previously described [25]. Porous 3DF scaffolds (Figs. 1B and D) were produced using a novel 3DF technique also described previously [26]. Previous thermal analysis studies have demonstrated that the compression molding and 3DF processing techniques described here do not result in changes of PEG molecular weight or PEGT/PBT composition [26] and, therefore, any differences seen between scaffolds in this

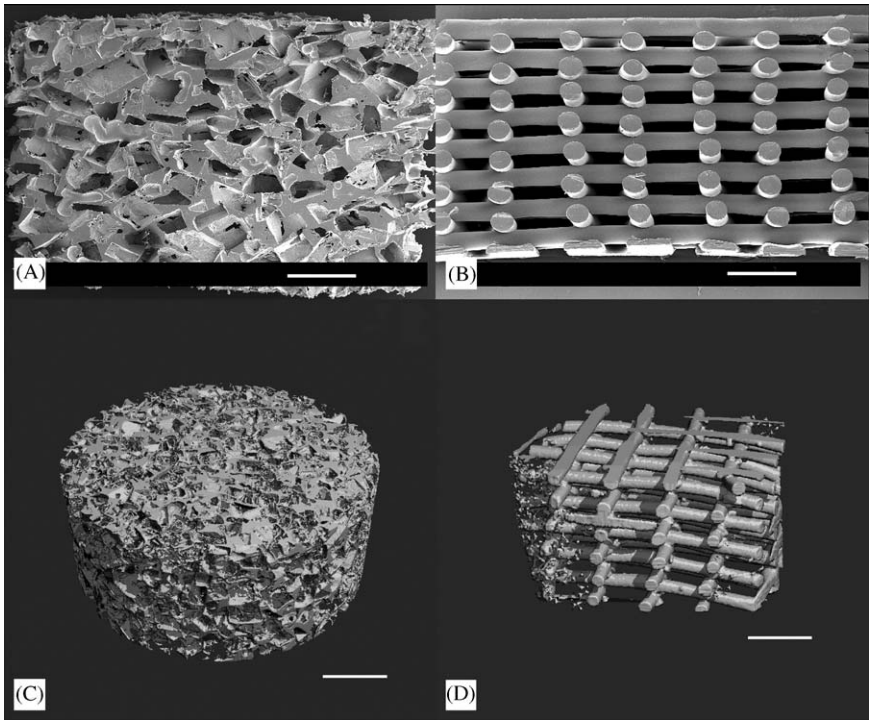

Fig. 1. Electron micrographs of CM (A) and 3DF (B) scaffolds. Three-dimensional reconstruction of CM (C) and 3DF (D) scaffolds from μCT scans. Scale bar represents 1 mm.

study could not be related to differences in scaffold composition.

Cylindrical scaffolds, 4×4 mm, were cored from the bulk porous CM and 3DF blocks and placed on surgical needles in 250 ml spinner flasks before being steam-sterilized (15 min, 121°C). Sterilized samples were incubated for at least 3 h in culture medium at 37°C to allow for scaffold hydration and serum protein adsorption prior to cell seeding.

2.2. Scaffold characterization

2.2.1. Micro-computed tomography (μCT)

Scaffolds were scanned using a desktop micro-computed tomography machine (μCT-40, Scanco Medical, Bassersdorf, Switzerland) at a resolution of 12 μm in all three spatial dimensions (X-ray voltage 45 kVp). Two hundred 2D slices (2048×2048 pixels) were scanned of every sample covering a height of 2.4 mm. The resulting gray-scale images were segmented and a threshold applied to extract the polymer architecture and then inverted to extract the pore volume (PV) architecture. This allowed 3D reconstruction (see Figs. 1C and D) of the total object volume (OV), scaffold volume (SV) and PV (OV = SV + PV) from stacked 2D images, which in turn could be analyzed to give information on porosity, surface area and pore size using algorithms previously developed for analyzing bone architecture [27–30]. Using a surface meshing technique [31], specific scaffold surface area was calculated (total surface area/SV). The pore size distribution was obtained by direct 3D measurement using a distance transformation technique [32], whereby the number of voxels within the total PV that could be filled by a sphere of a given diameter D_{pore} were measured (Fig. 2B). The average pore diameter was obtained by taking the mean over all sphere diameters.

To characterize the scaffold accessibility, an algorithm was designed (Scanco Medical, Bassersdorf, Switzerland) to mimic mercury intrusion porosimetry [33]. In other words, by starting at the periphery of the scaffold and working inwards, at a given sphere diameter, D_{int}, the amount of accessible PV was measured. Using a distance transformation [32], the local diameter, D, at every point within the PV was determined. Following a thresholding operation, the volume of pores with a local sphere diameter smaller than D_{int} were suppressed. All components of this thresholded structure not connected to the 'outside air' were then discarded using a component labeling operation. The volume of the resulting pore structure was determined and then plotted to produce a graph of the accessible PV versus interconnecting pore diameter D_{int} (Fig. 2A).

In addition to μCT, scaffold porosity was also determined using mass/volume techniques according to

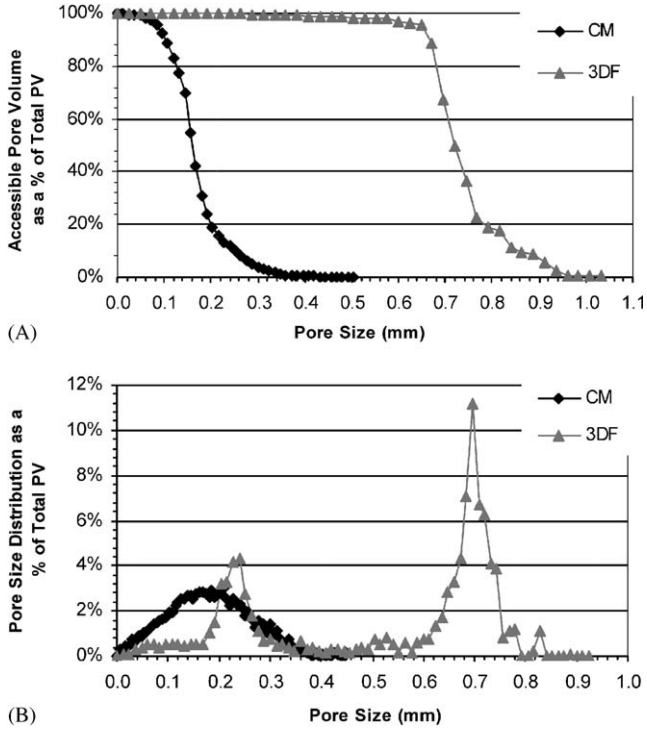

Fig. 2. Accessible PV distribution (A) and pore size distribution (B) for CM and 3DF scaffolds as was assessed based on μCT scans.

the following relationship:

$$\text{Vol\% porosity measured} = (1 - V_s/V_T) \times 100\%,$$

where V_s (mm^3) is the apparent SV (= polymer volume) given by m/ρ, where m and ρ are equal to the mass of the dry scaffold (g) and the polymer density ($\rho_{300/55/45} = 1.25 \times 10^{-3}$ g/cm^3), respectively. The total SV V_T (mm^3) was given by $\pi d^2 h/4$, where d and h are equal to the scaffold diameter (mm) and scaffold height (mm), respectively.

2.3. Mechanical characterization

To characterize the mechanical properties of scaffolds with varying architecture dynamic compression tests were carried out under wet conditions and compared with native AC tissue, as explained previously [26].

2.4. Cell isolation and culture

Chondrocytes were isolated from AC of the femoral condyles of 6-months-old bovine calves as previously described [34]. Isolated chondrocytes were seeded (3 million per scaffold) on the cylindrical (4×4 mm) scaffolds in culture medium (HEPES (Invitrogen)-buffered DMEM (Invitrogen) supplemented with 10% FCS (Sigma-Aldrich), 0.2 mM ascorbic acid 2-phosphate (Invitrogen), 0.1 mM non-essential amino

acids (Sigma-Aldrich), 0.4 mM proline (Sigma-Aldrich), 100 U/ml penicillin (Invitrogen), and 100 μg/ml streptomycin (Invitrogen)). Cell seeding and tissue culture were carried out in spinner flasks (Bellco Glass) stirred at 60 rpm, and contained at 37°C in a humidified 5% CO_2 incubator for up to 42 days. Culture medium was replaced every 2–3 days. This study reports the evaluation of a total of 230 scaffolds (excluding controls containing no cells), divided over two independent experiments.

2.5. In vivo implantation

Constructs cultured for 14 days as described above, were implanted in subcutaneous pockets of 6-week old nude mice (HdCpb:NMRI-nu, Harlan, The Netherlands). Animals were sacrificed at 7, 14, 21 and 28 days after implantation (i.e. 21, 28, 35 and 42 days after seeding), and constructs were processed histologically and biochemically, as described below.

2.6. Histology

Samples ($n = 3$ per time point) were taken after 3, 7, 14, 21 and 35 days after seeding and fixed overnight in 0.14 M cacodylate buffer (pH = 7.2–7.4) containing 0.25% glutaraldehyde (Merck) and subsequently dehydrated in a graded ethanol series. Samples were then embedded in glycol methacrylate (Merck) and cut using a microtome to yield 5 μm thick sections. Sections were stained with hematoxylin (Sigma-Aldrich) and fast green (Merck) for cells and with safranin-O (Sigma-Aldrich) for glycosaminoglycans (GAG).

2.7. Scanning electron microscopy (SEM)

Samples ($n = 3$ per time point) were taken after 3 days in vitro and after 14 days in vitro and an additional 21 days in vivo. Constructs were fixed and dehydrated as described above and critical point dried from liquid carbon dioxide using a Balzers CPD 030 Critical Point Dryer. Dried tissue-cultured samples or as-produced scaffolds were then sputter-coated (Cressingdon) with a thin gold layer and studied in a Philips XL 30 environmental scanning electron microscope (ESEM).

2.8. Immunohistochemistry

Constructs ($n = 3$ per time point) were taken after 14 days in vitro and an additional 21 days in vivo. Samples were embedded in an optimal cutting temperature (OCT) compound (Tissue-Tek) and cryo-sectioned to yield 5 μm thick sections, which were fixed in acetone for 8 min. Collagen type II was immunolocalized using an Animal Research Kit (Dako) in combination with a collagen type II antibody (1:200, II-II6B3, Developmental Studies Hybridoma Bank). After digestion for 20 min with 0.025% trypsin-EDTA (Invitrogen) at room temperature, samples were rinsed with PBS (Invitrogen) and incubated with peroxidase block for 5 min. Subsequently, the biotinylated primary antibody was applied for 15 min and rinsed with PBS. Streptavin-peroxidase was then applied for 15 min. After rinsing with PBS, the staining was visualized using DAB-solution for 5 min. Counter staining was performed with hematoxilin (Sigma-Aldrich).

2.9. Biochemical assays

Constructs ($n = 3$ per time point) were taken after 3, 14, 21, 28, 35 or 42 days and digested overnight at 56°C in a solution containing proteinase K, pepstatin A and iodoacetiamide (Sigma-Aldrich). Quantification of total DNA was done by Cyquant dye kit (Molecular Probes) using a spectrofluorometer (Perkin-Elmer). The amount of GAG was determined spectrophotometrically after reaction with dimethylmethylene blue dye (DMMB, Sigma-Aldrich) [35]. Intensity of color change was quantified immediately in a microplate reader (EL 312e Bio-TEK Instruments) by measuring absorbance at 520 nm. The amount of GAG was calculated using a standard of chondrotin sulphate B (Sigma-Aldrich). Total collagen was determined by measuring the amount of hydroxyproline present in each construct. Aliquots of proteinase K digest to be evaluated for hydroxyproline were hydrolyzed in 6 N HCl at 110°C for 16 h. The hydrolyzate was assayed for hydroxyproline using methods that have been described in detail elsewhere [36].

2.10. Statistics

Statistical significance was assessed by one-way analysis of variance (ANOVA) followed by a Student–Newman–Kuels posthoc test using Sigma Stat software (Jandal Corp.) with $p < 0.05$ as the criteria for statistical significance.

3. Results and discussion

3.1. Scaffold characterization

The two processing techniques used in this study, compression molding/particle leaching and 3DF, enabled fabrication of porous polymer scaffolds (Figs. 1A–D) with reproducible and comparable porosities. The vol% porosity based on mass–volume techniques was in the same range as the values obtained by 3D μCT analysis (Table 1). The specific scaffold surface area was 55.6 and 16.5/mm for CM and 3DF scaffolds, respectively. Both CM and 3DF scaffolds were ~100% interconnected, however CM scaffolds had a considerably

Table 1
Structural and mechanical characterization of PEGT/PBT scaffold architecture and AC

Sample	Measured vol% porosity		Surface area/unit vol.	Avg. pore size (D_{pore})	Dynamic stiffness at 0.1 Hz (MPa)
	m/V (%)	μCT (%)	μCT (mm^{-1})	μCT (μm)	
CM	75.6±1.9	81.8	55.6	182	1.72±0.33
3DF	70.2±1.8	77.6	16.5	525	4.33±0.52
Bovine AC [26]					4.10±1.57
Human AC (0.1 Hz) [45]					4.50

lower cut-off value (i.e. a pore size at which accessibility dropped below 90%) of ~120 μm compared with a ~680 μm cut-off value in 3DF scaffolds (Fig. 2A). The average pore size for CM scaffolds was 182 μm, but was substantially higher for 3DF scaffolds, namely 525 μm (Fig. 2B). For the CM scaffold the pore sizes approximated a Poisson distribution around an average of 182 μm, whilst, due to the layered organizational structure, two separate peaks were observed for the 3DF scaffolds (Fig. 2B). This was related to the fiber diameter dependent pore size in the z-direction (~200 μm) compared with pores generated in the $x-y$ plane based on a 1 mm fiber spacing (i.e. ~700 μm pore size).

The PV of 3DF scaffolds could be considered as a collection of continuous straight channels, unlike tortuous path of channels in CM scaffolds, which contained dead ends and narrow interconnections. Due to the tortuous pore structure and the lower average pore size in CM scaffolds, pores could be easily blocked with cells during seeding (“filtration effect”), thus preventing further cell access to the inner regions. Within the organized PV of 3DF scaffolds, the filtration effect would be less likely to occur and the diffusion distance would also be reduced.

It has been demonstrated that the effective diffusion coefficient within a scaffold is proportional to the porosity and inversely proportional to the tortuosity of the route through the pores that the substrate encounters [37]. Therefore, given that CM and 3DF scaffolds have similar porosity but different tortuosity, the effective diffusion coefficient of constructs based on 3DF scaffolds would be higher and nutrient transport would thus be enhanced in comparison to constructs based on CM scaffolds.

3.2. Cell density of TE constructs

After 3 days, DNA content per mg construct (proportional to the number of cells per wet weight) was slightly but significantly higher for the CM constructs (Fig. 3). This was likely related to their higher surface area per unit volume available for cell attachment compared with 3DF scaffolds (Table 1). Furthermore, the filtration effect within the tortuous pore structure was a plausible cause for the higher cell numbers observed on the outside of CM constructs (not shown). At the time of implantation at 14 days, however, there were no significant differences in overall cell number between CM and 3DF scaffolds. After 35 and 42 days, DNA/mg construct was significantly lower in in vivo cultures and was likely due to increased cartilaginous matrix deposition compared with in vitro cultures.

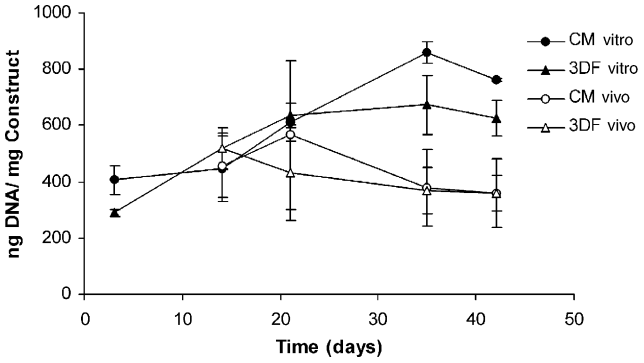

Fig. 3. DNA content of CM and 3DF constructs cultured in vitro and in vivo as assessed by CyQuant dye kit.

In addition, cell numbers in CM constructs after 35 and 42 days in vitro culture was slightly but significantly higher in comparison to 3DF constructs, possibly due to the higher surface area per unit volume available for cell proliferation within CM constructs. No differences in cell density between scaffold architectures were observed in vivo.

3.3. GAG content

After 3 days of culture in spinner flasks, cells were distributed throughout both scaffolds (Figs. 4A and B), however, particularly for CM scaffolds, more cells were present at the periphery (not shown). Safranin-O staining demonstrated that GAG, as a measure of cartilaginous tissue formation, was already present at this early time point. During the first 14 days of culture, tissue developed within the scaffolds and staining for GAG increased in both constructs (Figs. 4C and D). Meanwhile, a layer of spindle shaped cells developed at the periphery of the constructs. This dense layer of cells,

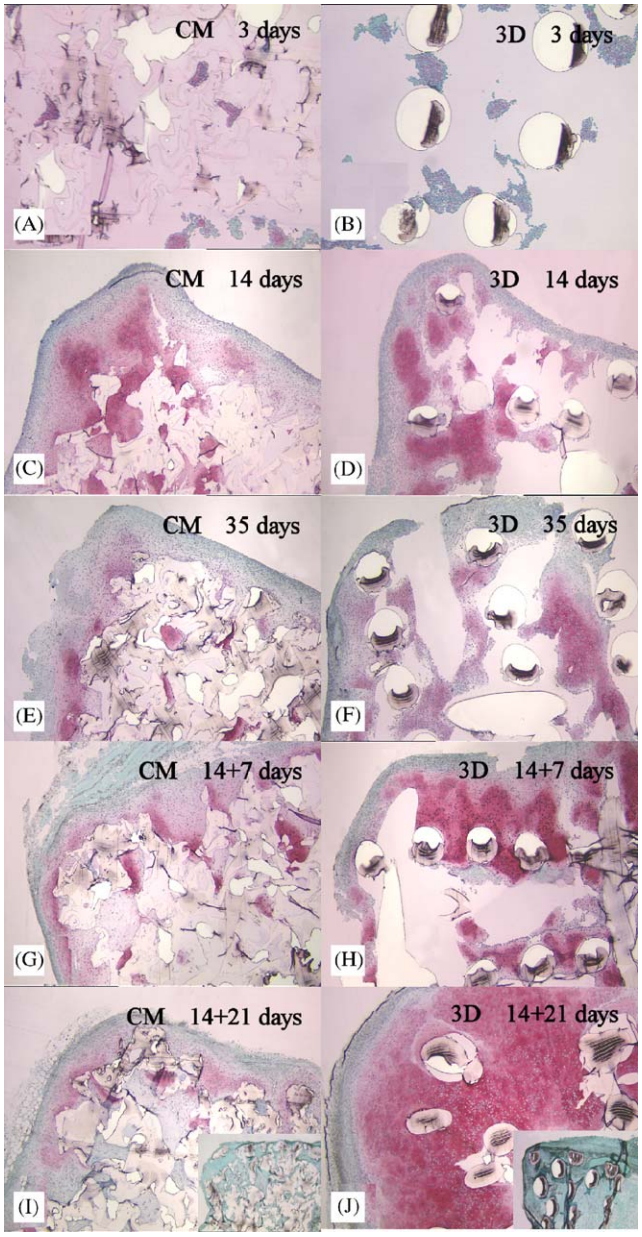

Fig. 4. Photomicrographs of safranin-O stained sections of CM (A, C, E, G, I) and 3DF (B, D, F, H, J) constructs cultured for 3 (A, B), 14 (C, D), 35 (E, F) days in vitro and 14 days in vitro and subsequently 7 (G, H) and 21 (I, J) days in vivo. Inset of I and J shows non-seeded controls. Scale bar represents 500 μm.

exhibiting a more fibroblast-like morphology than a differentiated chondrocyte morphology, could possibly have hampered nutrient transport into the construct. Prolonged dynamic culture in vitro did not result in further increase of cartilaginous tissue (Figs. 4E and F), and no difference in staining for GAG was observed between the two scaffold types. However, subcutaneous implantation in pockets on the back of nude mice yielded more intense staining for GAG within 3DF constructs 7 days after implantation (14 + 7 days) (Fig. 4H). Even more neo-cartilage tissue had developed after 21 days implantation (14 + 21 days), displaying a distinct chondrocytic morphology (Fig. 4J). In contrast, no additional production of GAG was observed within CM constructs following subcutaneous implantation (Figs. 4G and I), demonstrating that within 3DF scaffolds implanted in vivo, a more favorable environment for cartilaginous matrix deposition was created.

While explants containing cultured chondrocytes appeared non-vascular, scaffolds implanted without cultured chondrocytes did not stain for GAG and were highly vascularized (inset Figs. 4I and J).

The changes in GAG content as observed by histological evaluation using safranin-O were confirmed by the DMMB assay (Figs. 5A and B). Again, no differences between scaffold architectures were observed for the amount of GAG produced per cell, or per mg construct, during the first 14 days in vitro (Figs. 5A and B). GAG content for both constructs increased from approximately 3 μg per mg construct on day 3, to 7 μg per mg construct on day 14, i.e. from about 8–14 mg GAG per mg DNA. Prolonged dynamic culture in vitro resulted in a slight decrease of GAG content, which was likely due to a low production rate in combination with diffusion of

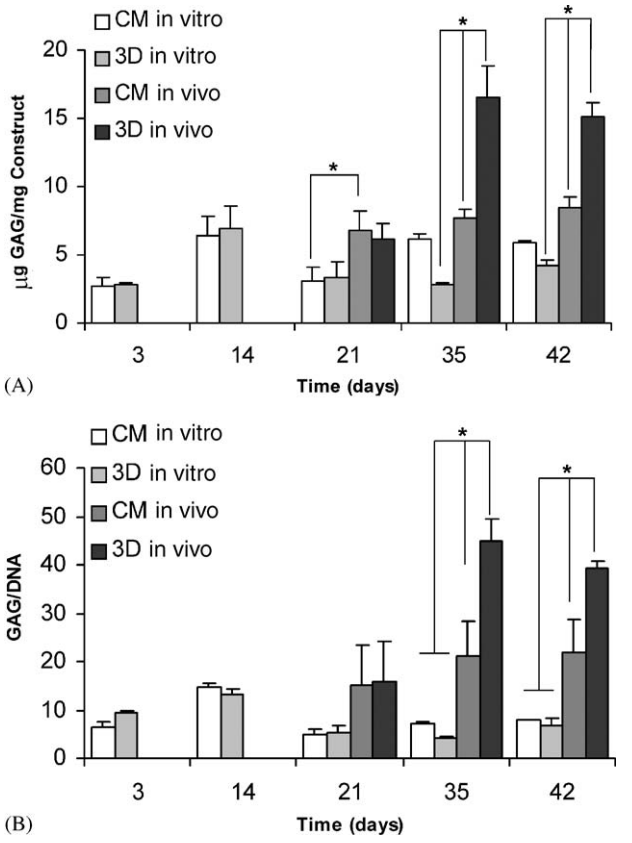

Fig. 5. GAG content of CM and 3DF constructs cultured in vitro and in vivo (μg GAG per mg construct (wet weight)(A) and mg GAG per mg DNA (B)). *Significant difference ($p < 0.05$) as assessed by DMMB staining.

GAG into the culture medium as was previously reported in other studies [38]. After subcutaneous implantation, GAG content increased, resulting in significantly higher GAG per cell values after 35 and 42 days compared with in vitro samples (Figs. 5A and B). Moreover, 3DF constructs contained significantly greater amounts of GAG (15.5 μg per mg construct, or 41 mg per mg DNA) compared with CM constructs (8 μg per mg construct, or 21 mg per mg DNA, respectively). Similarly, Freed et al. [39] demonstrated that neo-tissue formed on fibrous PGA scaffolds had a higher GAG content compared to spongeous PLLA scaffolds. However, that experiment did not clarify if the enhanced GAG formation was attributed to the scaffold architecture or the composition.

Previous studies in vitro using PGA-based constructs exhibited a higher GAG content (7–11 μg GAG per mg construct [2,39,40]) in comparison to those reported in this study for PEGT/PBT-based constructs (3–8.5 μg GAG per mg construct). In addition, upon implantation of these constructs in subcutaneous pockets in nude mice about 20 μg per mg construct was produced within 6 weeks, whereas in the present study we observed 15.5 μg GAG per mg 3DF-based construct. It should be noted, however, that in contrast to PGA, PEGT/PBT copolymers have a much slower degradation [41]. Consequently, a considerable volume of the construct will still be taken up by the biomaterial after 6 weeks and the formed neo-tissue will have an actual higher GAG content if normalized to tissue volume.

Although extensive cartilaginous tissue deposition was observed within 3DF scaffolds in vivo, considerably less cartilaginous tissue formed in vitro and no difference between the two architectures was observed. Thus, in vitro, further cell redifferentiation and concomitant ECM formation was limited by factors other than scaffold architecture. The conditions, which favored cartilage formation in vivo, were likely related to the presence of specific host-derived growth factors [42,43] and the absence of the dense fibrous cell layer present at the periphery of in vitro cultured constructs.

3.4. SEM

SEM confirmed histological observations that cells had attached and spread on the PEGT/PBT constructs (Figs. 6A and B) after 3 days. CM constructs cultured for 14 days in particular exhibited pores filled with fibroblast-like cells (Fig. 6C), whereas, following subcutaneous implantation, sparsely distributed round cells embedded in a ECM, a typical feature of hyaline cartilage tissue, were observed in both scaffolds as shown for the 3DF scaffold (Fig. 6D). Filamentous secretions, similar to those observed on hyaluronic acid-based fibrous scaffolds [44], were present on both scaffold types. However, in accordance with histology, 3DF constructs exhibited homogeneous formation of dense ECM throughout the internal pores, whereas more areas with spindle shaped fibroblast-like cells were observed in CM constructs. In addition, few internal pores within CM constructs were completely filled with ECM. SEM analysis confirmed that cartilaginous tissue formation in vivo was enhanced on 3DF scaffolds.

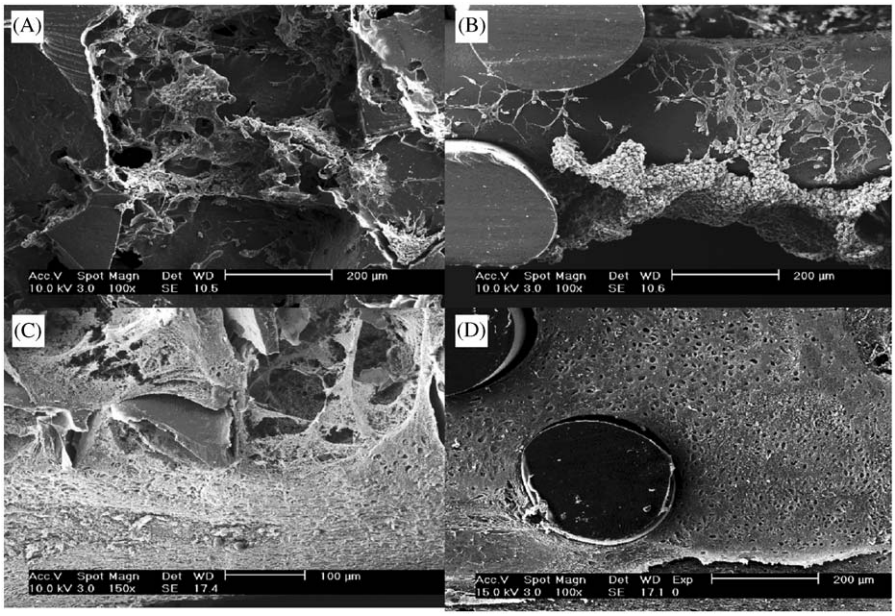

Fig. 6. Electron photomicrographs of CM (A, C) and 3DF (B, D) constructs after 3 days of in vitro culture (A, B) and 14 days of culture (C) and 14 days of in vitro culture and, subsequently, 21 days in vivo (D).

3.5. Collagen content

Total collagen content was assessed using the hydroxyproline assay. Collagen content did not change after 14 days of in vitro culture, whereas a significant increase was observed following in vivo implantation (Fig. 7). Although significantly more collagen per mg construct was produced in vivo in comparison to in vitro, no significant differences were observed between the two scaffold types at any of the time points assessed. Furthermore, total collagen production by bovine chondrocytes on fibrous PGA scaffolds cultured in spinner flasks for 6 weeks was reported to be approximately 3 times higher than for PEGT/PBT scaffolds used in this study [2,40].

Given that the hydroxyproline assay cannot discriminate between collagen types (i.e. type I and II), qualitative immunohistochemical assay was performed on samples maintained in vitro for 14 days and subsequently implanted for 21 days in vivo. Staining for collagen type II, a specific component of the hyaline cartilage extra-cellular matrix, could be demonstrated in both constructs, however, expression was never present at the peripheral edges of the constructs (Figs. 8A and B), but distributed homogeneously throughout the inner matrix (Figs. 8C and D).

Although differences in collagen type II content may be present between CM and 3DF constructs, using the qualitative immunohistochemical staining, we did not observe an effect of scaffold architecture on the formation of collagen type II within the present study. Similarly, LiVecchi et al. [14] demonstrated that the amount of type II collagen was not influenced by the pore size (ranging between 117 and 334 μm) of porous hydrophilic and hydrophobic high-density polyethylene (HDPE) matrices.

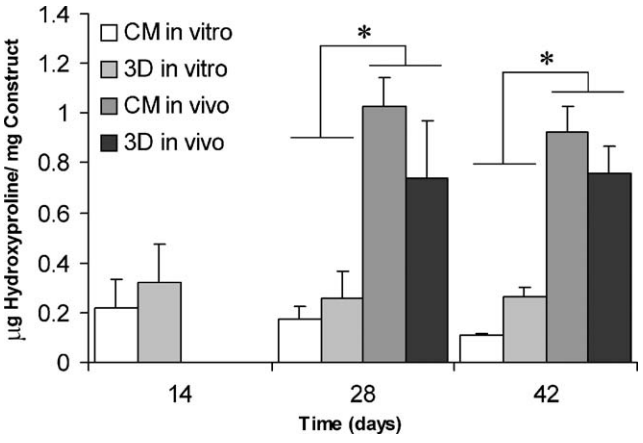

Fig. 7. Hydroxyproline content (as a measure of total collagen) of CM and 3DF constructs cultured in vitro and in vivo (μg hydroxyproline per mg construct (wet weight)).

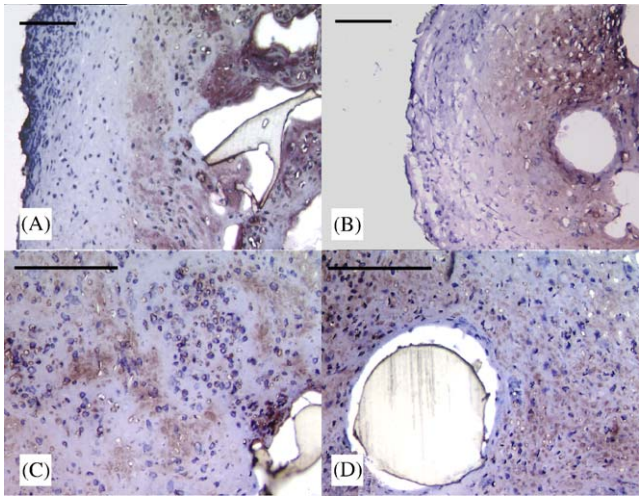

Fig. 8. Immunolocalization of collagen type II in the periphery (A, B) and center (C, D) of CM (A, C) and 3DF (B, D) constructs cultured 14 days in vitro and, additionally, 21 days in vivo. Scale bar represents 150 μm. Collagen type II was localized mainly within the center of the constructs.

3.6. Mechanical characterization

Dynamic compression tests were performed under wet conditions in order to characterize the mechanical stability of hydrated CM and 3DF architectures compared with native AC tissue. The dynamic stiffness (0.1 Hz) of 3DF scaffolds (4.33 MPa) was higher than for CM scaffolds (1.72 MPa) even though overall porosity was similar and pore size was significantly higher in 3DF scaffolds (Table 1). This was likely due to the organized fiber structure present within 3DF scaffolds compared with the irregular tortuous pores generated by particulates in CM scaffolds. 3DF scaffolds compared favorably with dynamic stiffness values measured for bovine AC [26] and human knee AC values obtained from literature [45] (Table 1).

Mechanical properties of fibrous PGA scaffolds were reported to be considerably lower than those of natural cartilage [46]. Although it has been shown in hyaluronic acid-based scaffolds, for example [47], that the presence of cells and deposited ECM can enhance the stability, the mechanical properties of constructs with cells will not be within the same range of those for native tissue. Due to the stability of PEGT/PBT scaffolds under dynamic mechanical compression scaffolds based on these architectures examined in this study would be suitable candidates for further in vivo assessment in a load bearing joint model. Moreover, it has been demonstrated that integration of immature in vitro cultured constructs to the surrounding AC was enhanced as opposed to mature constructs [48], and this may be particularly relevant in AC repair strategies that involve early implantation of cell-seeded scaffolds. Under this environment, these constructs could support

in vivo loading conditions whilst simultaneously exposing cells and neo-tissue to specific stimuli present in the in vivo environment.

4. Conclusion

To the best of our knowledge, no data has been reported in the literature that specifically demonstrates the effect of pore architecture, in particular pore accessibility and pore tortuosity, on the formation of neo-cartilage tissue. In the present study we evaluated two ~100% interconnected porous PEGT/PBT scaffolds, a compression-molded/particle-leached sponge (CM), and a novel 3D-deposited fiber (3DF) scaffold.

In vivo significantly more cartilaginous tissue was formed within 3DF constructs compared to CM constructs and collagen type II was found present regardless of scaffold type. In vitro, however, culture conditions did not support extensive cartilaginous tissue formation and consequently no differences were observed between the two scaffold architectures. Although GAG and total collagen content were reported to be higher for fibrous PGA-based constructs, these will not, in contrast to PEGT/PBT-based constructs, possess mechanical properties in the range of natural cartilage.

In conclusion, within 3DF PEGT/PBT scaffolds with a less tortuous and more accessible PV, an environment is created in vivo that enhances matrix deposition. Therefore, tissue-engineered constructs based on these scaffolds hold particular promise for treatment of AC defects.

Acknowledgements

The authors gratefully acknowledge Dr. I. Martin for his comments regarding this manuscript, Dr. Andres Laib (Scanco Medical AG, Bassersdorf, Switzerland) for assistance with μCT analysis as well as funding from the European Commission (FP5 project "Scafcart" G5RD-CT-1999-00050).

The collagen type II monoclonal antibody (developed by T.F. Linsenmayer) was obtained from the Developmental Studies Hybridoma Bank developed under the auspices of the NICHD and maintained by The University of Iowa, Department of Biological Science, Iowa City, IA 52242, USA.

References

[1] Buckwalter JA, Mankin HJ. Instructional Course Lectures, The American Academy of Orthopaedic Surgeons—articular cartilage. Part II: degeneration and osteoarthrosis, repair, regeneration, and transplantation. J Bone Jt Surg Am 1997;79:612–32.

[2] Freed LE, Hollander AP, Martin I, Barry JR, Langer R, Vunjak-Novakovic G. Chondrogenesis in a cell–polymer–bioreactor system. Exp Cell Res 1998;240:58–65.

[3] Obradovic B, Meldon JH, Freed LE, Vunjak-Novakovic G. Glycosaminoglycan deposition in engineered cartilage: experiments and mathematical model. AIChE J 2000;46:1860–71.

[4] Grimshaw MJ, Mason RM. Bovine articular chondrocyte function in vitro depends upon oxygen tension. Osteoarthritis Cartilage 2000;8:386–92.

[5] Malda J, Rouwkema J, Martens DE, le Comte P, Riesle J, Tramper J, van Blitterswijk CA. Oxygen gradients in tissue engineered PEGT/PBT cartilaginous constructs: modeled and measured. Biotechnol Bioeng 2004;86:9–18.

[6] Kellner K, Liebsch G, Klimant I, Wolfbeis OS, Blunk T, Schulz MB, Gopferich A. Determination of oxygen gradients in engineered tissue using a fluorescent sensor. Biotechnol Bioeng 2002;80:73–83.

[7] Lanza RP, Langer R, Vacanti J. Principles of tissue engineering. London: Academic Press; 2000.

[8] Vunjak-Novakovic G, Freed LE, Biron RJ, Langer R. Effects of mixing on tissue engineered cartilage. AIChE J 1996;42:850–60.

[9] Pei M, Solchaga LA, Seidel J, Zeng L, Vunjak-Novakovic G, Caplan AI, Freed LE. Bioreactors mediate the effectiveness of tissue engineering scaffolds. FASEB J 2002;16:1691–4.

[10] Mauck RL, Soltz MA, Wang CC, Wong DD, Chao PH, Valhmu WB, Hung CT, Ateshian GA. Functional tissue engineering of articular cartilage through dynamic loading of chondrocyte-seeded agarose gels. J Biomech Eng 2000;122:252–60.

[11] Gooch KJ, Blunk T, Courter DL, Sieminski AL, Bursac PM, Vunjak-Novakovic G, Freed LE. IGF-I and mechanical environment interact to modulate engineered cartilage development. Biochem Biophys Res Commun 2001;286:909–15.

[12] Nehrer S, Breinan HA, Ramappa A, Shortkroff S, Young G, Minas T, Sledge CB, Yannas IV, Spector M. Canine chondrocytes seeded in type I and type II collagen implants investigated in vitro. J Biomed Mater Res 1997;38:95–104.

[13] Bhardwaj T, Pilliar RM, Grynpas MD, Kandel RA. Effect of material geometry on cartilagenous tissue formation in vitro. J Biomed Mater Res 2001;57:190–9.

[14] LiVecchi AB, Tombes RM, LaBerge M. In vitro chondrocyte collagen deposition within porous HDPE: substrate microstructure and wettability effects. J Biomed Mater Res 1994;28:839–50.

[15] Woodfield TBF, Bezemer JM, Pieper JS, van Blitterswijk CA, Riesle J. Scaffolds for tissue engineering of cartilage. Crit Rev Euk Gene Exp 2002;12:207–35.

[16] Hutmacher DW. Scaffolds in tissue engineering bone and cartilage. Biomaterials 2000;21:2529–43.

[17] Zein I, Hutmacher DW, Tan KC, Teoh SH. Fused deposition modeling of novel scaffold architectures for tissue engineering applications. Biomaterials 2002;23:1169–85.

[18] Murphy WL, Dennis RG, Kileny JL, Mooney DJ. Salt fusion: an approach to improve pore interconnectivity within tissue engineering scaffolds. Tissue Eng 2002;8:43–52.

[19] Li S, de Wijn JR, Li J, Layrolle P, de Groot K. Macroporous biphasic calcium phosphate scaffold with high permeability/porosity ratio. Tissue Eng 2003;9:535–48.

[20] Putnam AJ, Mooney DJ. Tissue engineering using synthetic extracellular matrices. Nat Med 1996;2:824–6.

[21] Sakkers RJ, de Wijn JR, Dalmeijer R, Brand R, van Blitterswijk CA. Evaluation of copolymers of polyethylene oxide and polybuthylene terephtalate (Polyactive): mechanical behaviour. Mater Med 1998;9:375–9.

[22] van Blitterswijk CA, van den Brink J, Leenders H, Bakker D. The effect of PEO ratio on degradation, calcification and bone-bonding of PEO/PBT copolymer (Polyactive). Cells Mater 1993;3:23–36.

[23] Bezemer JM, Grijpma DW, Dijkstra PJ, van Blitterswijk CA, Feijen J. A controlled release system for proteins based on poly(ether ester) block-copolymers: polymer network characterization. J Control Release 1999;62:393–405.
[24] Deschamps AA, Claase MB, Sleijster WJ, de Bruijn JD, Grijpma DW, Feijen J. Design of segmented poly(ether ester) materials and structures for the tissue engineering of bone. J Control Release 2002;78:175–86.
[25] Du C, Klasens P, Haan RE, Bezemer J, Cui FZ, de Groot K, Layrolle P. Biomimetic calcium phosphate coatings on PolyActive 1000/70/30. J Biomed Mater Res 2002;59:535–46.
[26] Woodfield TBF, Malda J, de Wijn J, Péters F, Riesle J, van Blitterswijk CA. Design of porous scaffolds for cartilage tissue engineering using a 3-dimensional fiber-deposition technique. Biomaterials 2004;25(18):4149–61.
[27] Ruegsegger P, Koller B, Muller R. A microtomographic system for the nondestructive evaluation of bone architecture. Calcif Tissue Int 1996;58:24–9.
[28] Muller R, Ruegsegger P. Micro-tomographic imaging for the nondestructive evaluation of trabecular bone architecture. Stud Health Technol Inform 1997;40:61–79.
[29] Laib A, Barou O, Vico L, Lafage-Proust MH, Alexandre C, Rugsegger P. 3D micro-computed tomography of trabecular and cortical bone architecture with application to a rat model of immobilisation osteoporosis. Med Biol Eng Comput 2000;38:326–32.
[30] Zeltinger J, Sherwood JK, Graham DA, Mueller R, Griffith LG. Effect of pore size and void fraction on cellular adhesion, proliferation, and matrix deposition. Tissue Eng 2001;7:557–72.
[31] Lorensen WE, Cline HE. Marching cubes: a high-resolution 3D surface construct algorithm. Comput Graph 1987;21:163–9.
[32] Hildebrand T, Rüegsegger P. A new method for the model independent assessment of thickness in three-dimensional images. J Microsc 1997;185:67–75.
[33] Abell AB, Willis KL, Lange DA. Mercury intrusion porosimetry and image analysis of cement-based materials. J Colloid Interface Sci 1999;211:39–44.
[34] Malda J, Grojec M, Martens DE, Tramper J, van Blitterswijk CA, Riesle J. Expansion of bovine chondrocytes on microcarriers enhances redifferentiation. Tissue Eng 2003;9:939–48.
[35] Farndale RW, Buttle DJ, Barrett AJ. Improved quantitation and discrimination of sulphated glycosaminoglycans by use of dimethylmethylene blue. Biochim Biophys Acta 1986;883:173–7.
[36] Morales TI, Woessner JF, Howell DS, Marsh JM, Le Maire WJ. A microassay for the direct demonstration of collagenolytic activity in Graafian follicles of the rat. Biochim Biophys Acta 1978;524:428–34.
[37] Whang K, Goldstick TK, Healy KE. A biodegradable polymer scaffold for delivery of osteotropic factors. Biomaterials 2000; 21:2545–51.
[38] Obradovic B, Carrier RL, Vunjak-Novakovic G, Freed LE. Gas exchange is essential for bioreactor cultivation of tissue engineered cartilage. Biotechnol Bioeng 1999;63:197–205.
[39] Freed LE, Marquis JC, Nohria A, Emmanual J, Mikos AG, Langer R. Neocartilage formation in vitro and in vivo using cells cultured on synthetic biodegradable polymers. J Biomed Mater Res 1993;27:11–23.
[40] Gooch KJ, Kwon JH, Blunk T, Langer R, Freed LE, Vunjak-Novakovic G. Effects of mixing intensity on tissue-engineered cartilage. Biotechnol Bioeng 2001;72:402–7.
[41] Deschamps AA, van Apeldoorn AA, Hayen H, de Bruijn JD, Karst U, Grijpma DW, Feijen J. In vivo and in vitro degradation of poly(ether ester) block copolymers based on poly(ethylene glycol) and poly(butylene terephthalate). Biomaterials 2004;25: 247–58.
[42] Takigawa M, Shirai E, Fukuo K, Tajima K, Mori Y, Suzuki F. Chondrocytes dedifferentiated by serial monolayer culture form cartilage nodules in nude mice. Bone Miner 1987;2: 449–62.
[43] Mallein-Gerin F, Ruggiero F, Garrone R. Proteoglycan core protein and type II collagen gene expressions are not correlated with cell shape changes during low density chondrocyte cultures. Differentiation 1990;43:204–11.
[44] Grigolo B, Lisignoli G, Piacentini A, Fiorini M, Gobbi P, Mazzotti G, Duca M, Pavesio A, Facchini A. Evidence for redifferentiation of human chondrocytes grown on a hyaluronan-based biomaterial (HYAff 11): molecular, immunohistochemical and ultrastructural analysis [in process citation]. Biomaterials 2002;23:1187–95.
[45] Treppo S, Koepp H, Quan EC, Cole AA, Kuettner KE, Grodzinsky AJ. Comparison of biomechanical and biochemical properties of cartilage from human knee and ankle pairs. J Orthop Res 2000;18:739–48.
[46] Ma PX, Schloo B, Mooney D, Langer R. Development of biomechanical properties and morphogenesis of in vitro tissue engineered cartilage. J Biomed Mater Res 1995;29:1587–95.
[47] Aigner J, Tegeler J, Hutzler P, Campoccia D, Pavesio A, Hammer C, Kastenbauer E, Naumann A. Cartilage tissue engineering with novel nonwoven structured biomaterial based on hyaluronic acid benzyl ester. J Biomed Mater Res 1998;42:172–81.
[48] Obradovic B, Martin I, Padera RF, Treppo S, Freed LE, Vunjak-Novakovic G. Integration of engineered cartilage. J Orthop Res 2001;19:1089–97.